

Charged Higgs boson production via cb -fusion at the Large Hadron Collider

J. Hernández-Sánchez* and C. G. Honorato†

*Fac. de Cs. de la Electrónica, Benemérita Universidad Autónoma de Puebla,
Apartado Postal 1152, 72570 Puebla, Puebla, México*

S. Moretti‡

*School of Physics and Astronomy, University of Southampton,
Highfield, Southampton SO17 1BJ, United Kingdom,
and Particle Physics Department, Rutherford Appleton Laboratory,
Chilton, Didcot, Oxon OX11 0QX, United Kingdom*

S. Rosado-Navarro§

*Fac. de Cs. Físico-Matemáticas, Benemérita Universidad Autónoma de Puebla,
Apartado Postal 1364, C.P. 72570 Puebla, Puebla, México*

(Dated: November 11, 2021)

We analyse the production of a light charged Higgs boson at the Large Hadron Collider (LHC) via the quark-fusion mechanism $c\bar{b} \rightarrow H^-$ considering the decay channel $H^- \rightarrow \tau\bar{\nu}_\tau$ in the final state. We study this process in the framework of the 2-Higgs Doublet Model Type III (2HDM-III) which assumes a four-zero texture in the Yukawa matrices and a general Higgs potential, wherein the two Higgs doublets coupling to both up and down fermions do generate Flavour Changing Neutral Currents (FCNCs) yet the latter can be controlled by the texture when flavour physics constraints are considered. We consider the parameter space of the model where this signal is enhanced and in agreement with both theoretical constraints and experimental data. In particular, we exploit the setup with lepton-specific-like Yukawa couplings and assess the LHC sensitivity to such H^\pm signals against the dominant irreducible and reducible backgrounds. We show that in our model $\text{BR}(H^\pm \rightarrow cb) \sim 0.1 - 0.2$ and $\text{BR}(H^\pm \rightarrow \tau\nu) \sim 0.7 - 0.9$ so that, under these conditions, the prospects for H^\pm detection in the 2HDM-III in the aforementioned production and decay channels are excellent assuming standard collider energy and luminosity conditions.

* jaime.hernandez@correo.buap.mx

† carlos.g.honorato@correo.buap.mx

‡ s.moretti@soton.ac.uk

§ sebastian.rosado@gmail.com

I. INTRODUCTION

In July 2012, at the Large Hadron Collider (LHC), a neutral spinless boson was discovered by both the ATLAS [1] and CMS [2] collaborations. This new state of Nature is very compatible with the Standard Model (SM) Higgs boson, so this theoretical construct seems to be fully established now. However, the SM-like limit of Electro-Weak Symmetry Breaking (EWSB) dynamics induced by a Higgs potential exists in several Beyond the SM (BSM) extensions of the Higgs sector. Notably, the 2-Higgs Doublet Model (2HDM) [3] in its Types I, II, III (or Y) and IV (or X), wherein Flavour Changing Neutral Currents (FCNCs) mediated by (pseudo)scalar Higgs states can be eliminated under discrete symmetries [3], is an intriguing BSM candidate, owing to the fact that it implements the same fundamental doublet structure of the SM (in fact, twice), assumes the same SM gauge symmetry group (i.e., $SU(3)_C \times SU(2)_L \times U(1)_Y$) and predicts a variety of new Higgs boson signatures that may be accessible at the LHC. In particular, of the eight degrees of freedom pertaining to a 2HDM, upon EWSB giving mass to the W^\pm and Z bosons, five survive as physical Higgs bosons: three are neutral (two CP-even, h and H with, conventionally, $M_h < M_H$ plus one CP-odd, A) while two are charged (H^\pm).

However, another, equally interesting kind of 2HDM is the one where FCFNs can be controlled by a particular texture in the Yukawa matrices [4]. In particular, in previous papers, we have implemented a four-zero texture in a scenario which we have called 2HDM Type III (2HDM-III) [5]. This model has a phenomenology that is very rich, which we studied at colliders in various instances [6]–[12], and some very interesting aspects, like flavour-violating quarks decays, which can be enhanced for neutral Higgs bosons with intermediate mass (i.e., below twice the Z boson mass).

Furthermore, in this model, the parameter space can avoid many of the current experimental constraints from flavour and Higgs physics and a light charged Higgs boson (i.e., with a mass below the top quark one) is allowed therein [11], so that the decay $H^- \rightarrow b\bar{c}$ is enhanced and its Branching Ratio (BR) can be dominant, above and beyond those of the customary (flavour diagonal) $s\bar{c}$ and $\tau\nu$ channels. (In fact, this channel has been also studied in a variety of Multi-Higgs Doublet Models (MHDMs) [13, 14], wherein the $\text{BR}(H^- \rightarrow b\bar{c}) \approx 0.7-0.8$ and one could obtain a considerable gain in sensitivity to the presence of a H^- by tagging the b quark.) Finally, we have also performed a study of the process $e^-p \rightarrow \nu_e H^- b$ followed by the signal $H^- \rightarrow b\bar{c}$ [6, 15, 16] at the Large Hadron electron Collider (LHeC), finding good detection prospects.

In this work, by exploiting the enhancement of the $H^- \rightarrow c\bar{b}$ vertex and building on the results previously presented in [11], we study the production of a light charged Higgs boson at the LHC via heavy-quark fusion, $b\bar{c} \rightarrow H^-$, followed by the decay $H^- \rightarrow \tau\bar{\nu}_\tau$ (hereafter, c.c. channels are always implied). We investigate these processes in the framework of the aforementioned 2HDM-III with so-called lepton-specific couplings and assess the LHC sensitivity to this production and decay dynamics against the leading background, i.e., the irreducible one $q\bar{q}' \rightarrow W^- \rightarrow \tau\bar{\nu}_\tau$, and the reducible noise produced by $gq' \rightarrow W^\pm q$ (with an additional jet) and $q\bar{q} \rightarrow W^+W^- \rightarrow l^+l^-\nu\nu$ (where one lepton escapes detection, given that we will be looking for leptonic decays of the τ in the signal. An up-to-date overview of charged Higgs boson phenomenology at the LHC can be found in Refs. [13, 17].

The plan of this paper is as follows. In the next section we describe the 2HDM-III. Then we introduce some benchmark configurations of it for the purpose of running a Monte Carlo (MC) simulation and discussing the ensuing signal and background results. Finally, we conclude.

II. THE 2HDM-III

In the 2HDM-III there are two (pseudo)scalar Higgs doublets, $\Phi_1^\dagger = (\phi_1^-, \phi_1^{0*})$ and $\Phi_2^\dagger = (\phi_2^-, \phi_2^{0*})$, with hypercharge +1, and both couple to all fermions. In order to control FCNCs, as intimated, we have implemented a specific four-zero texture as an effective flavour theory in the Yukawa sector, so that a discrete symmetry is not necessary [10, 11]. Then the $SU(2)_L \times U(1)_Y$ invariant scalar potential should be the most general one:

$$\begin{aligned} V(\Phi_1, \Phi_2) = & \mu_1^2(\Phi_1^\dagger\Phi_1) + \mu_2^2(\Phi_2^\dagger\Phi_2) - \left(\mu_{12}^2(\Phi_1^\dagger\Phi_2 + h.c.) \right) \\ & + \frac{1}{2}\lambda_1(\Phi_1^\dagger\Phi_1)^2 + \frac{1}{2}\lambda_2(\Phi_2^\dagger\Phi_2)^2 + \lambda_3(\Phi_1^\dagger\Phi_1)(\Phi_2^\dagger\Phi_2) + \lambda_4(\Phi_1^\dagger\Phi_2)(\Phi_2^\dagger\Phi_1) \\ & + \left(\frac{1}{2}\lambda_5(\Phi_1^\dagger\Phi_2)^2 + \lambda_6(\Phi_1^\dagger\Phi_1)(\Phi_1^\dagger\Phi_2) + \lambda_7(\Phi_2^\dagger\Phi_2)(\Phi_1^\dagger\Phi_2) + h.c. \right). \end{aligned} \quad (1)$$

Here, we have assumed all parameters to be real, including the Vacuum Expectation Values (VEVs) of the (pseudo)scalar fields, therefore there is no CP-Violating (CPV) dynamics. Furthermore, note that, typically, the λ_6 and λ_7 parameters are absent when a discrete symmetry is considered (e.g., $\Phi_1 \rightarrow \Phi_1$ and $\Phi_2 \rightarrow -\Phi_2$).

Other than the physical Higgs masses (M_h, M_H, M_A and $M_{H^\pm}^\pm$), further independent parameters of the 2HDM are the mixing angles α (related to the mass matrix of the CP-even sector) and β (where $\tan \beta$ is the ratio of the two VEVs of the 2HDM). In our model, 2HDM-III, a four-zero texture is implemented as the mechanism that controls FCNCs and the terms proportional to λ_6 and λ_7 are kept. Herein, the EW parameter $\rho = M_W^2/M_Z^2 \cos^2 \theta_W$ can receive corrections at one-loop level proportional to the difference between the charged Higgs and CP-even/odd masses, but it is not sensitive to the value of λ_6 and λ_7 [9]. In particular, when the difference of the scalars masses $M_{H^\pm} - M_A (M_{H^\pm} - M_H)$ is large, the subadjacent custodial symmetry (twisted custodial symmetry) is broken. Then, a survival model to this EW observable is realised when $\rho \approx 1$ [18–20]. In general, the above mass splitting appears also in the expressions of the oblique parameters S, T and U (the so-called EW Precisions Observables (EWPOs)) [21], so they should be reconciled too with the corresponding experimental bounds [22]. Hence, the benchmark scenarios chosen for our model in the next section will be in agreement with these EW measurements.

For our model the Yukawa Lagrangian is given by [11]:

$$\mathcal{L}_Y = - \left(Y_1^u \bar{Q}_L \tilde{\Phi}_1 u_R + Y_2^u \bar{Q}_L \tilde{\Phi}_2 u_R + Y_1^d \bar{Q}_L \Phi_1 d_R + Y_2^d \bar{Q}_L \Phi_2 d_R + Y_1^l \bar{L}_L \tilde{\Phi}_1 l_R + Y_2^l \bar{L}_L \tilde{\Phi}_2 l_R \right), \quad (2)$$

where $\tilde{\Phi}_{1,2} = i\sigma_2 \Phi_{1,2}^*$. The fermion mass matrices after EWSB are: $M_f = \frac{1}{\sqrt{2}} (v_1 Y_1^f + v_2 Y_2^f)$, $f = u, d, l$, and both Yukawa matrices Y_1^f and Y_2^f have the aforementioned four-zero texture form and are Hermitian. Once diagonalisation is done, $\bar{M}_f = V_{fL}^\dagger M_f V_{fR}$, with $\bar{M}_f = \frac{1}{\sqrt{2}} (v_1 \tilde{Y}_1^f + v_2 \tilde{Y}_2^f)$, and $\tilde{Y}_i^f = V_{fL}^\dagger Y_i^f V_{fR}$, we can get from the product $V_q Y_n^q V_q^\dagger$ the rotated matrix \tilde{Y}_n^q as [11]:

$$[\tilde{Y}_n^q]_{ij} = \frac{\sqrt{m_i^q m_j^q}}{v} [\tilde{\chi}_n^q]_{ij} = \frac{\sqrt{m_i^q m_j^q}}{v} [\chi_n^q]_{ij} e^{i\vartheta_{ij}^q}, \quad (3)$$

where the χ s are unknown dimensionless parameters of the model. Following the procedure of [11], one can get the interactions of the charged Higgs bosons with the fermions,

$$\mathcal{L}^{\bar{f}_i f_j \phi} = - \left\{ \frac{\sqrt{2}}{v} \bar{u}_i (m_{d_j} X_{ij} P_R + m_{u_i} Y_{ij} P_L) d_j H^+ + \frac{\sqrt{2} m_{l_j}}{v} Z_{ij} \bar{\nu}_L l_R H^+ + h.c. \right\}, \quad (4)$$

where X_{ij}, Y_{ij} and Z_{ij} are defined as follows¹:

$$X_{ij} = \sum_{l=1}^3 (V_{\text{CKM}})_{il} \left[X \frac{m_{d_l}}{m_{d_j}} \delta_{lj} - \frac{f(X)}{\sqrt{2}} \sqrt{\frac{m_{d_l}}{m_{d_j}}} \tilde{\chi}_{lj}^d \right], \quad (5)$$

$$Y_{ij} = \sum_{l=1}^3 \left[Y \delta_{il} - \frac{f(Y)}{\sqrt{2}} \sqrt{\frac{m_{u_l}}{m_{u_i}}} \tilde{\chi}_{il}^u \right] (V_{\text{CKM}})_{lj}, \quad (6)$$

$$Z_{ij}^l = \left[Z \frac{m_{l_i}}{m_{l_j}} \delta_{ij} - \frac{f(Z)}{\sqrt{2}} \sqrt{\frac{m_{l_i}}{m_{l_j}}} \tilde{\chi}_{ij}^l \right], \quad (7)$$

where $f(a) = \sqrt{1+a^2}$ and the parameters X, Y and Z are arbitrary complex numbers that can be linked to $\tan \beta$ or $\cot \beta$ when $\chi_{ij}^f = 0$ [11], so that it is then possible to recover the standard four types of 2HDM (see Tab. I)². Furthermore, the Higgs-fermion-fermion couplings ($\phi f f$) in the 2HDM-III can be written as $g_{2\text{HDM-III}}^{\phi f f} = g_{2\text{HDM-any}}^{\phi f f} + \Delta g$, where $g_{2\text{HDM-any}}^{\phi f f}$ is the coupling $\phi f f$ in any of the 2HDMs with discrete symmetry and Δg is the contribution of the four-zero texture. Lastly, we also point out that this Lagrangian can represent a Multi-Higgs Doublet Model (MHDM) or an Aligned 2HDM (A2HDM) with additional flavour physics in the Yukawa matrices [10, 11].

III. BENCHMARK SCENARIO

We have constrained our model using flavour and Higgs physics (i.e., the measurements of the SM-like Higgs boson discovered at the LHC plus the exclusions emerging from void searches for additional Higgs states at any collider) as

¹ Hereafter, V_{CKM} is the Cabibbo-Kobayashi-Maskawa matrix.

² Hence, we will refer to these 2HDM-III ‘incarnations’ as 2HDM-III like- χ scenarios, where $\chi = \text{I, II, X and Y}$.

2HDM-III	X	Y	Z
2HDM Type I	$-\cot \beta$	$\cot \beta$	$-\cot \beta$
2HDM Type II	$\tan \beta$	$\cot \beta$	$\tan \beta$
2HDM Type X	$-\cot \beta$	$\cot \beta$	$\tan \beta$
2HDM Type Y	$\tan \beta$	$\cot \beta$	$-\cot \beta$

TABLE I. The parameters X , Y and Z of the 2HDM-III defined in the Yukawa interactions when $\chi_{ij}^f = 0$ so as to recover the standard four types of 2HDM.

well as EWPOs and theoretical bounds (like vacuum stability, unitarity and perturbativity). While we do not discuss the theoretical constraints (as they are a simple application of textbook methods), we dwell here at some length on all the experimental ones, with the intent of emphasising those applicable to a charged Higgs state.

Specifically, the model is found in agreement with flavour physics constraints by taking into account the analyses performed in Refs. [10, 11, 23], where the parameter space of the 2HDM-III is constrained by leptonic and semi-leptonic meson decays, like the inclusive decays $B \rightarrow X_s \gamma$, $B_0 - B_0$ as well as $K_0 - K_0$ mixing and $B_s \rightarrow \mu^+ \mu^-$ transitions. Here, the Yukawa texture used in the model plays a relevant role in the amplitudes of the mesonic decays, altogether allowing for the possibility to obtain a light charged Higgs state, of order 100 GeV or so, in the case of Type X couplings (with all other Yukawa cases being more constrained in terms of M_{H^\pm}).

Further, as for constraints from the SM-like Higgs boson measurements, we consider the impact at one loop-level of charged Higgs bosons on the radiative decays $h \rightarrow \gamma\gamma$ and γZ , as detailed in [9]. For this analysis, some of the most recent experimental data from the LHC are considered, namely, from Refs. [24–28]. Once again, the Yukawa texture is involved in the couplings of the charged Higgs boson with fermions in the loop and low masses for a Type X Yukawa structure are allowed.

As for the current bounds on the mass of a charged Higgs boson from direct searches at present and past colliders, we have considered the following, recalling that for a light charged Higgs boson the main production mode at lepton machines is via $e^+ e^- \rightarrow H^+ H^-$ while at hadron colliders is via $gg \rightarrow t\bar{b}H^- + \text{c.c.}$ (so that, for $M_{H^\pm} < m_t$, the latter correspond to top pair production and decay via a charged Higgs boson, i.e., $t \rightarrow bH^+$).

- LEP limits. For the mass of the charged Higgs boson, the LEP collaborations have finally established a universal lower bound at 78.6 GeV [29].
- Tevatron limits. For a charged Higgs boson with a mass between 90 GeV and 160 GeV, CDF and D0 established a bound for the the $\text{BR}(t \rightarrow bH^+)$ of $\approx 20\%$ taking $\text{BR}(H^+ \rightarrow c\bar{s}) = 1$ or $\text{BR}(H^+ \rightarrow \tau^+ \nu) = 1$ [30–32].
- LHC limits. For the case $\text{BR}(H^+ \rightarrow \tau^+ \nu) = 1$ in the range of masses varying from 80 GeV to 160 GeV, the CMS experiment has established a $\text{BR}(t \rightarrow bH^+) = 2 - 3\%$ as upper limit. Meanwhile, for the mass range 90 GeV to 160 GeV with $\text{BR}(H^+ \rightarrow c\bar{s}) = 1$, both ATLAS and CMS set $\text{BR}(t \rightarrow bH^+) \approx 20\%$ as a maximum [22]. Finally, assuming $\text{BR}(H^+ \rightarrow c\bar{b}) = 1$, in the mass range 90 GeV to 150 GeV, the CMS collaboration has set an upper limit of $\text{BR}(t \rightarrow H^+ b) = 0.5 - 0.8\%$ [33].

As for EW data, we have fixed the oblique parameter $U = 0$, because this is suppressed with respect to the parameters S and T when a scale for new physics (just) above the EW regime is considered [22], taking $S = 0.02 \pm 0.07$ and $T = 0.06 \pm 0.06$.

Upon the application of all limits above, the following parameter space region roughly survives and is analysed here: $M_h = 125$ GeV (thus with h being the SM-like Higgs boson), $M_A = 100$ GeV, $180 \text{ GeV} < M_H < 260$ GeV and $100 \text{ GeV} < M_{H^\pm} < 170$ GeV, with $0.1 < \cos(\beta - \alpha) < 0.5$. Over such an expanse of parameter space, we consider four scenarios, each in turn being an incarnation of our 2HDM-III: like-I (where one Higgs doublet couples to all fermions); like-II (where one Higgs doublet couples to the up-type quarks and the other to the down-type quarks); like-X (also called IV or "Lepton-specific", where the quark couplings are Type I and the lepton ones are Type II); like-Y (also called III or "Flipped", where the quark couplings are Type II and the lepton ones are Type I).

For a light charged Higgs boson, in the 2HDM-III, the most important decay channels are $H^\pm \rightarrow sc$ and bc , when $Y \gg X, Z$ (like-I scenario), $X, Z \gg Y$ (like-II scenario) or $X \gg Y, Z$ (like-Y scenario), in which cases the mode $H^\pm \rightarrow bc$ receives a substantial enhancement coming from the four-zero texture implemented in the Yukawa matrices, so one can even get a $\text{BR}(H^- \rightarrow b\bar{c}) \approx 0.95$. However, this does not happen for $H^\pm \rightarrow \tau\nu$, which is the decay we must rely on in order to extract a charged Higgs boson signal in the hadronic environment of the LHC, specifically, assuming a leptonic decay of the τ . For the case $Z \gg X, Y$ (like-X scenario), the decay channel $H^- \rightarrow \tau\bar{\nu}_\tau$ is maximised, reaching a BR of 90% or so [11], while not penalising the $H^\pm \rightarrow bc$ mode excessively, so that, in turn, the

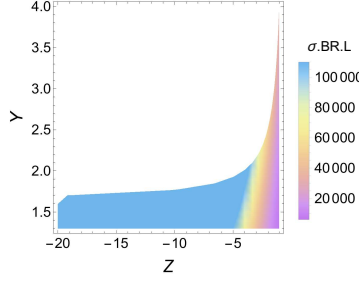


FIG. 1. Event rates for our BP at parton-level for $M_{H^\pm} = 120$ GeV and $X = -1/Z$, assuming $\sqrt{s} = 13$ TeV and $L = 36.1$ fb $^{-1}$.

production $c\bar{b} \rightarrow H^+$ can reach a considerable cross section. In fact, a typical configuration is $\text{BR}(H^\pm \rightarrow \tau\nu) \approx 0.9$ and $\text{BR}(H^\pm \rightarrow cb) \approx 0.1$. Guided by the parameter scan performed in [8], we finally adopt the following Benchmark Point (BP) in order to analyse by MC simulation at the LHC the process $c\bar{b} \rightarrow H^+ \rightarrow \tau\bar{\nu}_\tau$, as it offers the most optimistic chances for detection.

- Scenario 2HDM-III like-X: $\cos(\beta - \alpha) = 0.5$, $\chi_{22}^u = 1$, $\chi_{23}^u = 0.1$, $\chi_{33}^u = 1.4$, $\chi_{22}^d = 1.8$, $\chi_{23}^d = 0.1$, $\chi_{33}^d = 1.2$, $\chi_{22}^\ell = -0.4$, $\chi_{23}^\ell = 0.1$, $\chi_{33}^\ell = 1$ with $Z \gg X, Y$. Further, we assume $M_h = 125$ GeV, $M_A = 100$ GeV, $M_H = 150$ GeV and $100 \text{ GeV} < M_{H^\pm} < 170$ GeV. In fact, eventually, given the significant signal-to-background rates obtained for a light charged Higgs boson state, we will push our analysis up to 1 TeV or so for its mass.

IV. NUMERICAL RESULTS

As already stressed, we will attempt to establish the signal $b\bar{c} \rightarrow H^- \rightarrow \tau\bar{\nu}_\tau$ at the LHC, by surpassing the results of Ref. [11], wherein a similar analysis was performed, although over a region of parameter space of the 2HDM-III which has largely been ruled out since, following the subsequent discovery of a SM-like Higgs boson at the LHC as well as the measurements of its properties therein. In fact, since that paper, also a myriad of void experimental searches for additional Higgs bosons were carried out by the LHC collaborations, which also impinge on the available 2HDM-III parameter space.

As intimated, the cross section for our signal process is too small in the 2HDM-III incarnations of Type I, II and Y, therefore only the Type X realisation is explored here. It was seen in our scan that its value is maximised for small X , so we fixed the latter to be $X = -1/Z$. The results of our scan over the plane (Y, Z) are presented in Fig. 1, in terms of the $\sigma(b\bar{c} \rightarrow H^-) \times \text{BR}(H^- \rightarrow \tau\bar{\nu}_\tau) \times L$ yield³, where $L = 36.1$ fb $^{-1}$ is the LHC luminosity at an energy of $\sqrt{s} = 13$ TeV, corresponding to the values used by the CMS collaboration in their $H^\pm \rightarrow \tau^\pm \nu_\tau$ decay channel analysis [34]. Here, we fix $M_{H^\pm} = 120$ GeV for reference. It is clear that the inclusive rate is very significant, the best point being $X = 0.04$, $Y = 1.6$, $Z = -20$, which produces $\approx 2.276 \times 10^6$ events.

In order to carry out our numerical analysis, we have used CalcHEP 3.7 [35] as parton level event generator, interfaced to the CTEQ6L1 Parton Distribution Functions (PDFs) [36] and to PYTHIA6 [37] for parton shower, hadronisation and heavy flavour decays while PGS [38] was the detector emulator, supplemented by a generic LHC parameter card. In particular, the detector parameters simulated were as follows. We considered a calorimeter coverage $|\eta| < 5.0$, with segmentation $\Delta\eta \times \Delta\phi = 0.087 \times 0.10$ (the number of division in η and ϕ were 320 and 200, respectively). Moreover, we used Gaussian energy resolution, with

$$\frac{\Delta E}{E} = \frac{a}{\sqrt{E}} \oplus b, \quad (8)$$

where $a = 0.5$ and $b = 0.03$ for both the Electro-Magnetic (EM) and hadron calorimeter resolution, with \oplus meaning addition in quadrature. The algorithm to perform jet finding was a “cone” one with jet radius $\Delta R = 0.5$. The calorimeter trigger cluster finding a seed(shoulder) threshold was 5 GeV(1 GeV). Further, the kinematic behaviour of the final state particles was mapped with the help of MadAnalysis5 [39].

For the MC analysis, six masses were selected for the charged Higgs boson: 120, 170, 200 400, 500 and 750 GeV. For each such values, the dominant background is the irreducible one induced by $q\bar{q}' \rightarrow W^\pm \rightarrow \tau\bar{\nu}_\tau$, even if M_{H^\pm} is

³ In fact, we use here a factorisation formula exploiting the charged Higgs boson in Narrow Width Approximation (NWA), given that it is very narrow. (This is done for calculation efficiency purposes.)

always significantly larger than M_{W^\pm} (indeed, in line with the findings of Ref. [11]). The aforementioned reducible backgrounds, $gq' \rightarrow W^\pm q$ and $q\bar{q} \rightarrow W^+W^- \rightarrow l^+l^-\nu\nu$, are smaller in comparison. However, all of these are included in our analysis. As previously stated, we will be looking for leptonic τ decays, so that the final state is $l + \cancel{E}_T$, where $l = e, \mu$ and \cancel{E}_T is the missing transverse energy. We placed no cuts on the latter while for both lepton and jets the following acceptance region in transverse momentum and rapidity was adopted: $p_T(l), p_T(j) > 10$ GeV and $|\eta(l)|, |\eta(j)| < 3$ with $\Delta R(j, l) > 0.5$. In fact, owing to QCD Initial State Radiation (ISR), there could be any number of jets in the final state, however, in our analysis, we will finally select events with at least one lepton and no jets.

Since the invariant mass of the final state is not reconstructible, as previously done [11], one can analyse the transverse mass $M_T(l) \equiv \sqrt{(E_l^T - \cancel{E}_T)^2 - (p_l^x + p_{miss}^x)^2 - (p_l^y + p_{miss}^y)^2}$, where $p_{l,miss}^x$ and $p_{l,miss}^y$ are located in the transverse plane, thus assuming that the proton beams are along the z -axis. In Fig. 2, the shape of the transverse mass is reconstructed at detector level without selection cuts, wherein both signal and background can be seen, which reinforces the fact that, at the differential level (e.g., for $m_{H^\pm} = 120$ and 170 GeV, although the situation is the same for any other mass), the potential Jacobian peak correlating to the charged Higgs boson mass is well beyond the background distribution. Hence, a careful signal selection will be proposed which preserves such a difference as much as possible. In particular, we will optimise this to the given value of the charged Higgs boson mass. That is, a trial and error approach will be assumed, wherein the M_{H^\pm} value is an input parameter to the kinematic analysis and the selection cuts adopted depend on it.

In order to fully define our selection, let us now investigate some relevant differential distributions that can be used to enhance the signal-to-background rate. (Notice that, for reasons of space, we will not show all charged Higgs mass values in each case.)

1. From the lepton and hadronic multiplicity plots, see Figs. 3 and 4, we require at least one lepton and impose no jets in our sample. (Here, we impose on both lepton and jets the acceptance region in transverse momentum and rapidity as already discussed: i.e., $p_T(l), p_T(j) > 10$ GeV and $|\eta(l)|, |\eta(j)| < 3$ with $\Delta R(j, l) > 0.5$.) Further, by looking at Fig. 5 (wherein the jet veto is applied), it can be seen that the cut $p_T(l) \geq 45$ GeV on the leptonic transverse momentum can be profitably adopted for all charged Higgs mass boson masses.
2. The missing transverse energy plots, Fig. 6, suggest the use of the following cuts: for $M_{H^\pm} = 120$ GeV, $40 \text{ GeV} \leq \cancel{E}_T \leq 70 \text{ GeV}$; for $M_{H^\pm} = 170$ GeV, $60 \text{ GeV} \leq \cancel{E}_T \leq 90 \text{ GeV}$; for $M_{H^\pm} = 200$ GeV, $70 \text{ GeV} \leq \cancel{E}_T \leq 105 \text{ GeV}$; for $M_{H^\pm} = 400$ GeV, $100 \text{ GeV} \leq \cancel{E}_T \leq 225 \text{ GeV}$; for $M_{H^\pm} = 500$ GeV, $90 \text{ GeV} \leq \cancel{E}_T \leq 270 \text{ GeV}$; for $M_{H^\pm} = 750$ GeV, $105 \text{ GeV} \leq \cancel{E}_T$.
3. The lepton pseudorapidity, Fig. 7, shows that an optimal cut can be defined for all charged Higgs boson masses as $|\eta(l)| \leq 1.2$.
4. The total energy, Fig. 8, shows that the following cuts can be efficient: for $M_{H^\pm} = 120, 170$ GeV, $E_T \geq 55$ GeV; for $M_{H^\pm} = 200$ GeV, $E_T \geq 60$ GeV; for $M_{H^\pm} = 400$ GeV, $E_T \geq 80$ GeV; for $M_{H^\pm} = 500$ GeV, $E_T \geq 75$ GeV; for $M_{H^\pm} = 750$ GeV, $E_T \geq 80$ GeV.
5. The transverse mass plots in Fig. 9 show that the last cuts to be defined can be as follows: for $M_{H^\pm} = 120$ GeV, $85 \text{ GeV} \leq M_T(l) \leq 125 \text{ GeV}$; for $M_{H^\pm} = 170$ GeV, $90 \text{ GeV} \leq M_T(l) \leq 175 \text{ GeV}$; for $M_{H^\pm} = 200$ GeV, $110 \text{ GeV} \leq M_T(l) \leq 205 \text{ GeV}$; for $M_{H^\pm} = 400$ GeV, $170 \text{ GeV} \leq M_T(l) \leq 405 \text{ GeV}$; for $M_{H^\pm} = 500$ GeV, $200 \text{ GeV} \leq M_T(l) \leq 505 \text{ GeV}$; for $M_{H^\pm} = 750$ GeV, $320 \text{ GeV} \leq M_T(l) \leq 755 \text{ GeV}$.

Following the above sequence of cuts, for which the signal and background responses can be found in Tab. II, we revisit in Fig. 10 the transverse mass distributions in the relevant peak regions. From these, the significances given in Tab. III can be extracted. In turn, from the latter, it can be concluded that the signal is strong enough to be detectable at the LHC over a very large mass range, covering both the light and heavy mass regime of the charged Higgs boson stemming from the 2HDM-III. In fact, by interpolating between the various charged Higgs boson masses used in the MC analysis, we can perform a continuous scan of the relevant 2HDM-III like-X parameter space surviving current theoretical and experimental limits and map the signal significances, obtained at $L = 36.1 \text{ fb}^{-1}$ via the above search channel, in terms of the 2HDM-III input parameters to which the latter is sensitive, i.e., $\tan\beta$, χ_{33}^l (via Y) and M_{H^\pm} . This is done in Fig. 11.

V. CONCLUSIONS

In summary, there exist significance chances to extract a charged Higgs boson signal at the LHC within the 2HDM-III scenario in its like-X incarnation, by searching for the production and decay channel $b\bar{c} \rightarrow H^- \rightarrow \tau\bar{\nu}_\tau$, wherein the

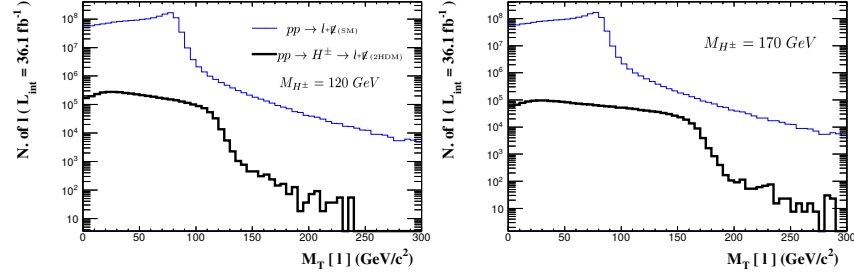


FIG. 2. Transverse mass plots for signal and background, for selected M_{H^\pm} choices of the former. No cuts are here applied.

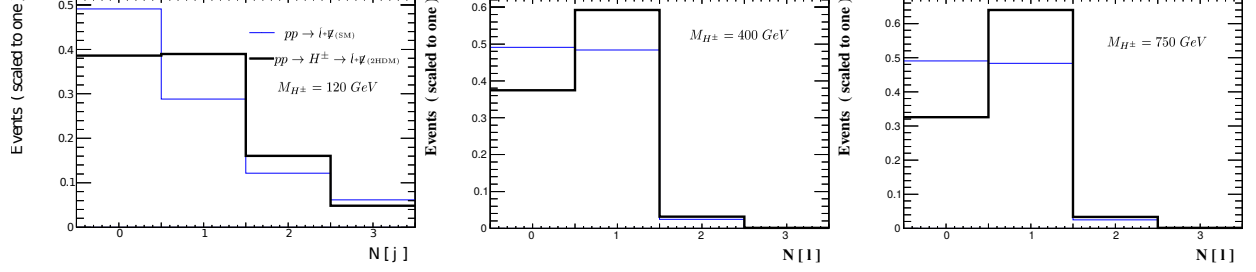


FIG. 3. Lepton multiplicity plots for signal and background, for selected M_{H^\pm} choices of the former, over the acceptance region for leptons and jets, in both transverse momentum as pseudorapidity.

τ is identified through its transitions into electrons/muons and corresponding neutrinos (the latter yielding transverse missing energy). This can be achieved by the end of Run 3 over a H^\pm mass interval ranging from 100 GeV or so up to the TeV scale. In order to obtain this, a dedicated selection procedure is required to be optimised around a tentative charged Higgs boson mass value. We have proven this to be very effective against the (dominant) background given by $b\bar{c} \rightarrow W^- \rightarrow \tau\bar{\nu}_\tau$ as well as the (subdominant) noise produced via $gq' \rightarrow W^\pm q$ and $q\bar{q}' \rightarrow W^+W^- \rightarrow l^+l^-\nu\nu$. Finally, we are confident that our results are realistic, as we have obtained these through a sophisticated MC analysis exploiting advanced computational tools. We are therefore looking forward to ATLAS and CMS adopting our recommended approach, so as to confirm or disprove the 2HDM-III hypothesis.

ACKNOWLEDGEMENTS

SM is financed in part through the NExT Institute and the UK STFC Consolidated grant ST/L000296/1. SM acknowledge support from the H2020-MSCA-RISE-2014 grant no. 645722 (NonMinimalHiggs). SR-N thanks the University of Southampton as well as Carleton University for hospitality while parts of this work were completed. JH-S and CH have been supported by SNI-CONACYT (México), VIEP-BUAP and PRODEP-SEP (México) under the grant ‘Red Temática: Física del Higgs y del Sabor’. SR-N acknowledges a scholarship from CONACYT (México).

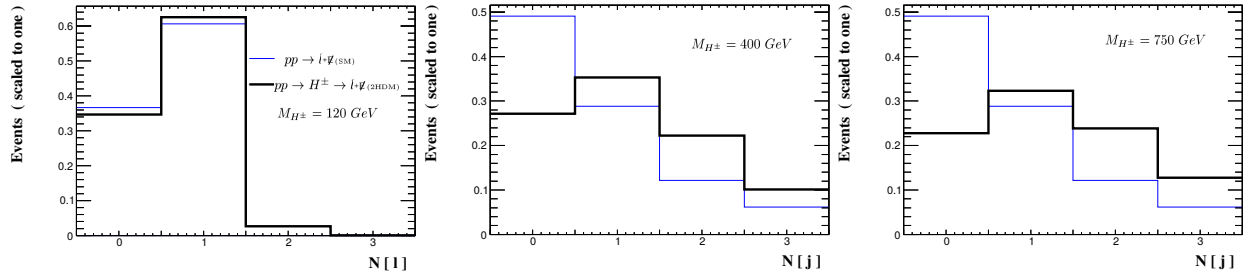


FIG. 4. Hadron multiplicity plots for signal and background, for selected M_{H^\pm} choices of the former, over the acceptance region for leptons and jets, in both transverse momentum and pseudorapidity.

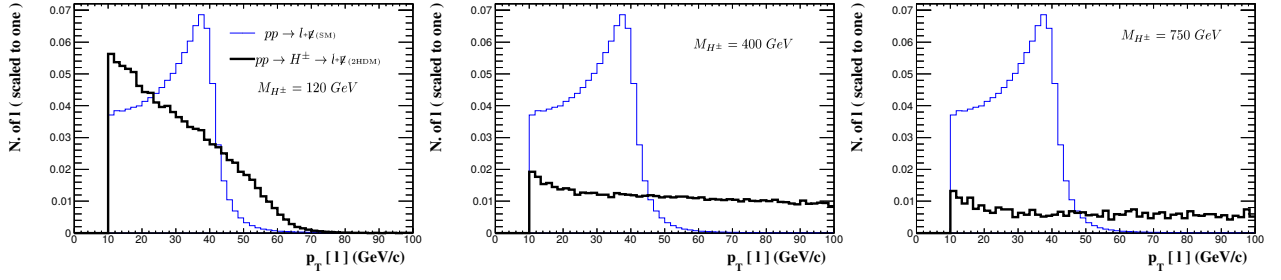


FIG. 5. Leptonic transverse momentum plots for signal and background, for selected M_{H^\pm} choices of the former, over the acceptance region for leptons and jets, in both transverse momentum as pseudorapidity. Further, jets are vetoed here.

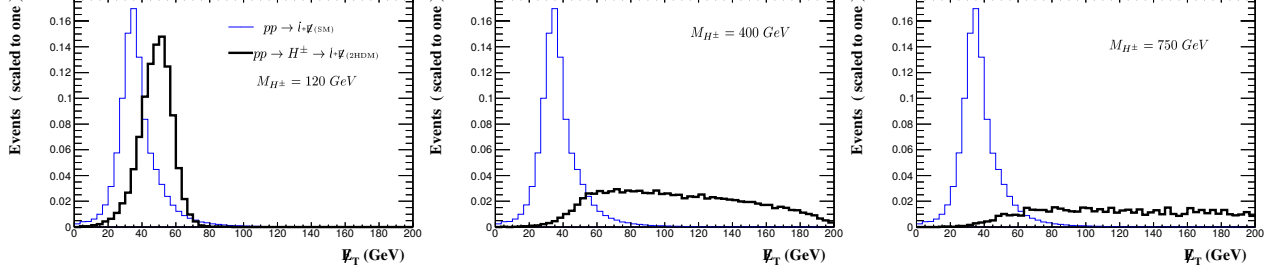


FIG. 6. Missing transverse energy plots for signal and background, for selected M_{H^\pm} choices of the former, over the acceptance region for leptons and jets, in both transverse momentum as pseudorapidity. Further, jets are vetoed here.

We all thank Professor Heather Logan for useful and constructive discussions in the beginning of this work.

-
- [1] G. Aad et. al. [ATLAS Collaboration], Phys. Lett. B **716**, 1 (2012) [arXiv:1207.7214[hep-ex]].
 - [2] S. Chatrchyan et. al. [CMS Collaboration], Phys. Lett. B **716**, 30 (2012) [arXiv: 1207.7235[hep-ex]].
 - [3] G. C. Branco, P. M. Ferreira, L. Lavoura, M. N. Rebelo, M. Sher and J. P. Silva, Phys. Rept. **516**, 1 (2012) [arXiv:1106.0034 [hep-ph]].
 - [4] H. Fritzsch and Z. z. Xing, Phys. Lett. B **555**, 63 (2003) [hep-ph/0212195].
 - [5] J. L. Díaz-Cruz, J. Hernández-Sánchez, S. Moretti, R. Noriega-Papaqui and A. Rosado, Phys. Rev. D **79**, 095025 (2009) [arXiv:0902.4490 [hep-ph]].
 - [6] J. Hernández-Sánchez, O. Flores-Sánchez, C. G. Honorato, S. Moretti and S. Rosado, PoS CHARGED **2016**, 032 (2017) [arXiv:1612.06316 [hep-ph]].
 - [7] J. Hernández-Sánchez, S. P. Das, S. Moretti, A. Rosado and R. Xoxocotzi-Aguilar, PoS DIS **2015**, 227 (2015) [arXiv:1509.05491 [hep-ph]].
 - [8] S. P. Das, J. Hernández-Sánchez, S. Moretti, A. Rosado and R. Xoxocotzi, Phys. Rev. D **94**, no. 5, 055003 (2016) [arXiv:1503.01464 [hep-ph]].

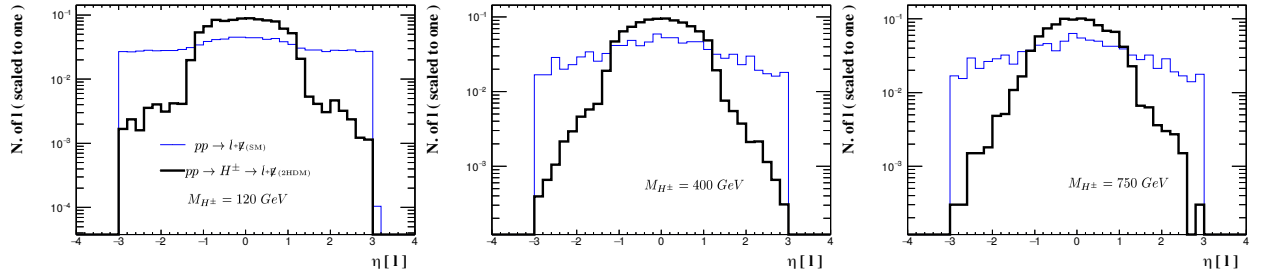


FIG. 7. Pseudorapidity plots for signal and background, for selected M_{H^\pm} choices of the former, over the acceptance region for leptons and jets, in both transverse momentum as pseudorapidity. Further, jets are vetoed here.

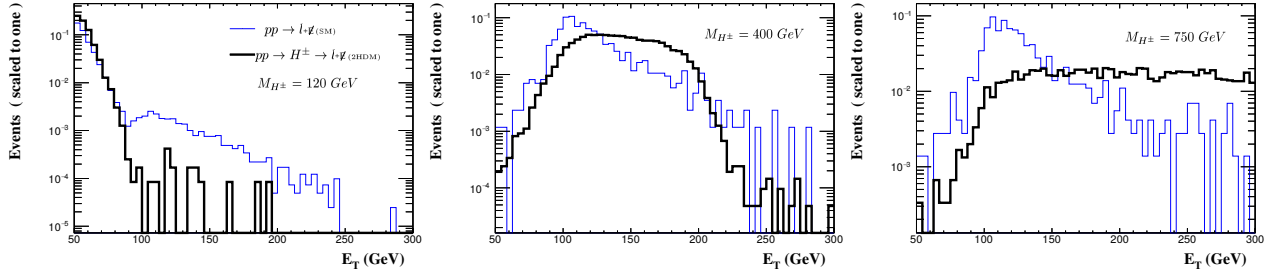


FIG. 8. Missing transverse energy plots for signal and background, for selected M_{H^\pm} choices of the former, over the acceptance region for leptons and jets, in both transverse momentum as pseudorapidity. Further, jets are vetoed here.

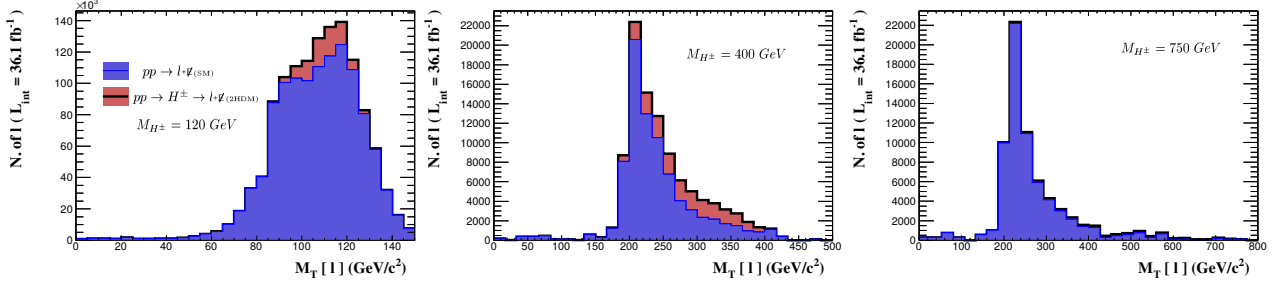


FIG. 9. Transverse mass plots for signal and background, for selected M_{H^\pm} choices of the former, after Cuts 1–4. Histograms are stacked here.

- [9] A. Cordero-Cid, J. Hernández-Sánchez, C. G. Honorato, S. Moretti, M. A. Pérez and A. Rosado, JHEP **1407**, 057 (2014) [arXiv:1312.5614 [hep-ph]].
- [10] O. Félix-Beltrán, F. González-Canales, J. Hernández-Sánchez, S. Moretti, R. Noriega-Papaqui and A. Rosado, Phys. Lett. B **742**, 347 (2015) [arXiv:1311.5210 [hep-ph]].
- [11] J. Hernández-Sánchez, S. Moretti, R. Noriega-Papaqui and A. Rosado, JHEP **1307**, 044 (2013) [arXiv:1212.6818 [hep-ph]].
- [12] J. Hernández-Sánchez, S. Moretti, R. Noriega-Papaqui and A. Rosado, PoS CHARGED **2012**, 029 (2012) [arXiv:1302.0083 [hep-ph]].
- [13] A. G. Akeroyd *et al.*, Eur. Phys. J. C **77**, no. 5, 276 (2017) [arXiv:1607.01320 [hep-ph]].
- [14] A. G. Akeroyd, S. Moretti and J. Hernández-Sánchez, Phys. Rev. D **85**, 115002 (2012) [arXiv:1203.5769 [hep-ph]].
- [15] O. Flores-Sánchez, J. Hernández-Sánchez, C. G. Honorato, S. Moretti and S. Rosado-Navarro, Phys. Rev. D **99**, no. 9, 095009 (2019) [arXiv:1811.05476 [hep-ph]].
- [16] O. Flores-Sánchez, J. Hernández-Sánchez, C. G. Honorato, S. Moretti and S. Rosado, PoS DIS **2019**, 094 (2019) [arXiv:1908.09405 [hep-ph]].
- [17] A. Arhrib, R. Benbrik, H. Harouiz, S. Moretti and A. Rouchad, doi:10.3389/fphy.2020.00039 [arXiv:1810.09106 [hep-ph]].
- [18] J. F. Gunion and H. E. Haber, Phys. Rev. D **67**, 075019 (2003) [hep-ph/0207010].
- [19] J.-M. Gerard and M. Herquet, Phys. Rev. Lett. **98**, 251802 (2007) [hep-ph/0703051 [HEP-PH]].
- [20] S. de Visscher, J. M. Gerard, M. Herquet, V. Lemaître and F. Maltoni, JHEP **0908**, 042 (2009) [arXiv:0904.0705 [hep-ph]].
- [21] S. Kanemura, Y. Okada, H. Taniguchi and K. Tsumura, Phys. Lett. B **704**, 303 (2011) [arXiv:1108.3297 [hep-ph]].
- [22] M. Tanabashi *et al.* (Particle Data Group), Phys. Rev. D **98**, 030001 (2018)

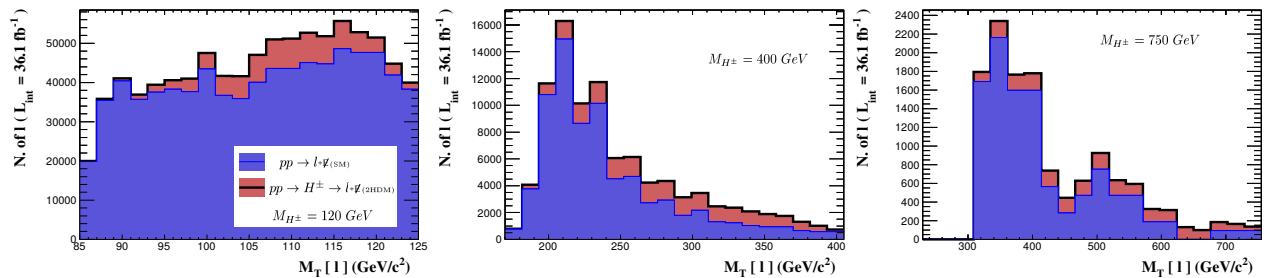


FIG. 10. Transverse mass plots for signal and background with all cuts taken into account, i.e., limited to the region used for the calculation of the significances.

M_{H^\pm}	Cut 1: $p_T(l)$	Cut 2: \cancel{E}_T	Cut 3: $ \eta(l) $	Cut 4: E_T	Cut 5: $M_T(l)$
120 GeV	≥ 45 GeV	≥ 40 GeV ≤ 70 GeV	≤ 1.2 GeV	≥ 55 GeV	≥ 85 GeV ≤ 125 GeV
Signal events	294136	237167	215684	85480	82147
Background events	27527568	7919086	3832807	1090294	795470
170 GeV	≥ 45 GeV	≥ 60 GeV ≤ 90 GeV	≤ 1.2 GeV	≥ 55 GeV	≥ 90 GeV ≤ 175 GeV
Signal events	290051	138676	124849	114334	113758
Background events	27527568	1282301	669345	568972	536547
200 GeV	≥ 45 GeV	≥ 70 GeV ≤ 105 GeV	≤ 1.2 GeV	≥ 60 GeV	≥ 110 GeV ≤ 205 GeV
Signal events	233230	94175	84981	80777	80453
Background events	27527568	627241	333826	304128	290406
400 GeV	≥ 45 GeV	≥ 100 GeV ≤ 225 GeV	≤ 1.2 GeV	≥ 80 GeV	≥ 170 GeV ≤ 405 GeV
Signal events	42612	22833	20864	20714	20578
Background events	27527568	146801	80449	78475	74904
500 GeV	≥ 45 GeV	≥ 90 GeV ≤ 270 GeV	≤ 1.2 GeV	≥ 75 GeV	≥ 200 GeV ≤ 505 GeV
Signal events	20674	14716	13292	13194	12021
Background events	27527568	238246	129132	124809	71238
750 GeV	≥ 45 GeV	≥ 105 GeV	≥ 80 GeV	≥ 1 GeV	≥ 320 GeV ≤ 755 GeV
Signal events	4381	3351	3049	3042	2279
Background events	27527568	124057	68043	66539	10714

TABLE II. Number of events after doing the multiplicity cuts of signal and background each cut described in the text, adopting the same sequence, $L = 36.1 \text{ fb}^{-1}$.

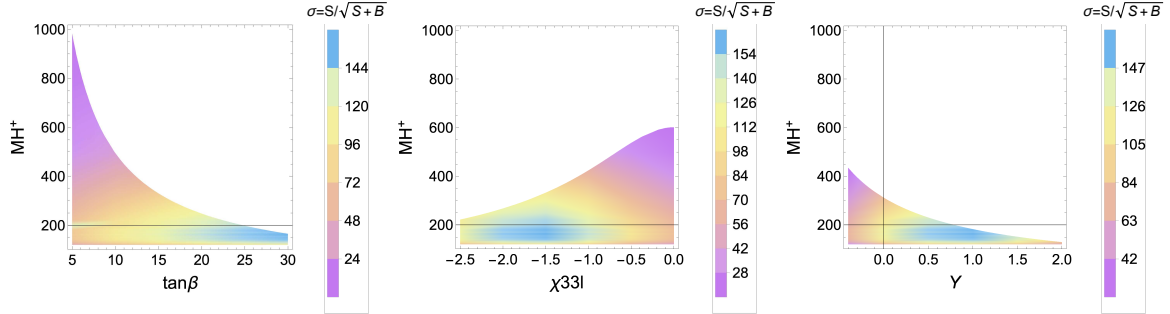


FIG. 11. Significance of our signal in terms of the most relevant parameters of the 2HDM-III like-X scenario.

- [23] A. Crivellin, C. Greub and A. Kokulu, Phys. Rev. D **87**, no. 9, 094031 (2013) [arXiv:1303.5877 [hep-ph]].
- [24] M. Aaboud *et al.* [ATLAS Collaboration], Phys. Lett. B **784**, 345 (2018) [arXiv:1806.00242 [hep-ex]].
- [25] M. Aaboud *et al.* [ATLAS Collaboration], Phys. Lett. B **786**, 114 (2018) [arXiv:1805.10197 [hep-ex]].
- [26] M. Aaboud *et al.* [ATLAS Collaboration], JHEP **1710**, 112 (2017) [arXiv:1708.00212 [hep-ex]].
- [27] A. M. Sirunyan *et al.* [CMS Collaboration], [arXiv:1809.10733 [hep-ex]].
- [28] A. M. Sirunyan *et al.* [CMS Collaboration], JHEP **1811**, 152 (2018) [arXiv:1806.05996 [hep-ex]].
- [29] G. Abbiendi *et al.* [ALEPH, DELPHI, L3, OPAL and LEP], Eur. Phys. J. C **73** (2013), 2463 doi:10.1140/epjc/s10052-013-2463-1 [arXiv:1301.6065 [hep-ex]].
- [30] B. Abbott *et al.* [D0 Collaboration], Phys. Rev. Lett. **82**, 4975 (1999) [hep-ex/9902028].
- [31] A. Abulencia *et al.* [CDF Collaboration], Phys. Rev. Lett. **96**, 042003 (2006) [hep-ex/0510065].
- [32] V. M. Abazov *et al.* [D0 Collaboration], Phys. Lett. B **682**, 278 (2009) [arXiv:0908.1811 [hep-ex]].
- [33] A. M. Sirunyan *et al.* [CMS Collaboration], JHEP **1811**, 115 (2018) [arXiv:1808.06575 [hep-ex]].

H^\pm mass (GeV)	Signal	Background	$S/\sqrt{S+B}$
120	82147	795470	87.688
130	111026	745095	119.994
140	138553	852330	139.189
150	133205	719156	144.282
155	123148	633444	141.578
160	131734	673010	146.849
165	133767	683161	147.999
170	113758	536547	141.067
175	117716	544818	144.621
180	121355	566716	146.299
200	80453	290406	132.111
220	79475	292568	130.297
250	73119	314654	117.420
300	38855	112403	99.906
400	20578	74904	66.597
500	12021	71238	41.66
750	2279.4	10714	19.997
800	1643.8	9586.2	15.511
1000	637.5	5263	8.299

TABLE III. Significances after the complete sequence of cuts described in the text with $L = 36.1 \text{ fb}^{-1}$.

- [34] A. M. Sirunyan *et al.* [CMS Collaboration], JHEP **1907**, 142 (2019) [arXiv:1903.04560 [hep-ex]].
- [35] A. Belyaev, N. D. Christensen and A. Pukhov, Comput. Phys. Commun. **184**, 1729 (2013) [arXiv:1207.6082 [hep-ph]].
- [36] J. Pumplin, D. R. Stump, J. Huston, H. L. Lai, P. M. Nadolsky and W. K. Tung, JHEP **0207**, 012 (2002) [hep-ph/0201195].
- [37] T. Sjöstrand, S. Mrenna and P. Z. Skands, JHEP **0605**, 026 (2006) [hep-ph/0603175].
- [38] J. Conway, R. Culbertson, R. Demina, B. Kilminster, M. Kruse, S. Mrenna, J. Nielsen, M. Roco, A. Pierce, J. Thaler and T. Wizansky, <http://conway.physics.ucdavis.edu/research/software/pgs/pgs4-general.htm>.
- [39] E. Conte, B. Fuks and G. Serret, Comput. Phys. Commun. **184**, 222 (2013) [arXiv:1206.1599 [hep-ph]].